Improved process control by surface temperature-controlled drying on the example of sweet potatoes

***Michael Bantle*[1], *Christian Kopp*[1], *Ingrid C. Claussen*[1]**

[1] Department of Energy Processes, SINTEF Energy Research,
NO-7465 Trondheim, Norway
Michael.Bantle@Sintef.no

Abstract
Convective drying of food has a big impact on the quality of the product in terms of sensory quality and energy consumption. The temperature of the product during the drying process is a major parameter since exceeding can cause damages to the product. The surface temperature of the product can be measured non-disruptive and contact-free with IR-sensors and this information is used as input parameter for the dryer control. A convective drying chamber was modified with modern sensors and a smart control system to control the surface temperature during the drying process and evaluate the influences on the product in terms of sensory quality parameters like shrinkage, deformation and colour alternation. The dehydration rate in the first drying period of the constant surface temperature-controlled methods is about 1.5 to 2.5 times faster than the conventional method where the air temperature is kept constant and the quality parameters are not significant affected.

Keywords*: Convective drying, Smart drying, Surface temperature, optical change, energy efficiency*

1 Introduction

During the convective drying process, the surface of the drying products develops the highest temperatures. Depending on the product, too high temperatures can damage the products surface which results in a reduced quality in terms of e.g. appearance and texture (Mujumdar, 2015). By using modern sensors and a smart controlling system, the surface temperature can be regulated to avoid too high temperatures and kept constant over the whole drying process. In this study, the influences of surface temperature controlled convective drying was tested with sweet potatoes and the influences in terms of drying speed, optical quality parameters like colour alternation, shrinkage and deformation is evaluated.

2 Material and method

2.1 Drying chamber

The experiments were executed in a convective drying chamber with a dimension of approximately 3m * 1.5m * 1m with a tray area of 50 m^2. The drying chamber is equipped with an electric heater to set the drying temperature, a ventilator to set the air velocity and a heat pump to set the relative humidity. To avoid any interruptions or influences of the drying process due to measuring, a test rack was built and placed within the drying chamber at a representative point in the middle of the drier trays with all relevant measuring devices attached. The camera system (UI-5240CP-C-HQ Rev.2, company iDS Imaging Development Systems, Germany) contained a built-in heater to avoid influences of the image quality due to the surrounding temperatures in the drying chamber. The illumination was a LED-bar light (LHF300-M12-WHI, company Stemmer Imaging, Germany) with a colour temperature of 6500K. The camera system was used to measure colour alternations and deformations like shrinkage. To obtain also the sidelong deformation of the sweet potatoes, a mirror was placed in a 45° angle next to the slices. The weight loss during the drying process was recorded with a scale (SB32000, company Mettler Toledo) and to measure the surface temperature, a pyrometer (IR thermo sensor) was placed over a representative potato slice. Each test series was done with 4 replicates.

2.2 Product preparation

The used drying products in this work were organic sweet potatoes (Ipomoea batatas), which were purchased in Norway at the local market. The sweet potatoes were stored in a refrigerator at 8°C during the whole experimental duration of 2 weeks. The sweet potatoes were cut in slices of 5 mm thickness using a bread cutter machine. The peel wasn't removed.
To measure the drying kinetics, 1000 g of the potato slices were placed on a drying grid which was placed on a scale inside the drying chamber. One of those slides was placed underneath the pyrometer to measure the representative surface temperature. For the optical measurement 6 slices were placed on the camera test rack.

2.3 Experimental Setup

Figure 1 shows the two used drying methods using the example of 30°C

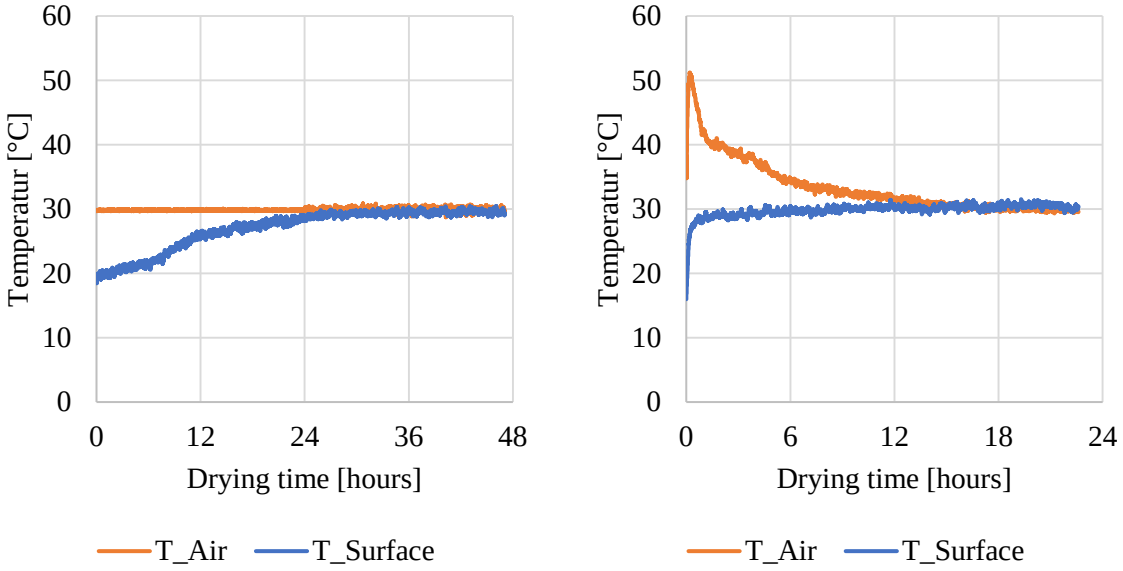

Figure 1: Temperature profile of air temp. controlled (left) and surface temp. controlled (right).

On the left side the temperature profile is shown, where the air temperature was kept constant, which can be considered as the classical method for convectional drying. The surface temperature is increasing during the drying process until it is reaching the temperature of the drying air.
On the right side a temperature profile of the surface temperature-controlled method is shown. This method keeps the temperature of the product surface constant and results in a higher air temperature in the beginning, which reduces during the drying process until it reaches the surface temperature. In this work the following experimental setups were used (see Table 1):

Table 1: Overview test series

Test name	Constant temperature	Temperature, T [°C]	Rel. humidity, RH [%]	Air velocity, v [m/s]
T20_Air	Air temp.	19.8 ± 0.2	32.1 ± 2.1	1.0 ± 0.05
T30_Air	Air temp.	29.8 ± 0.2	29.4 ± 1.8	1.1 ± 0.04
T40_Air	Air temp.	39.6 ±0.1	28.0 ± 2.2	1.1 ± 0.03
T20_Surface	Surface temp.	19.9 ± 0.5	33.1 ± 1.5	1.0 ± 0.07
T30_Surface	Surface temp.	29.8 ± 1.0	28.5 ± 3.1	1.1 ± 0.06
T40_Surface	Surface temp	39.4 ± 1.5	28.9 ± 3.3	1.1 ± 0.05

The relative humidity and air velocity for the different tests are shown in Table 1 and are not varying significantly; hence the determined differences in drying dynamics will be mainly caused by the drying temperature.

2.4 Shrinkage and deformation

During the drying process, an image was taken by the camera every 5 minutes and analysed afterwards with a self-developed program using the OpenCV libraries (Bradski, 2000).
The shrinkage was determined by measuring the slice area in pixels for every image which results in a relative percental area shrinkage according the following equation:

$$Shrinkage(t) = \frac{Area(t)}{Area_{t0}} \quad (1)$$

The deformation was determined by the ratio of the actual slice area and its smallest enclosure circle/rectangle area as shown in Figure 2.

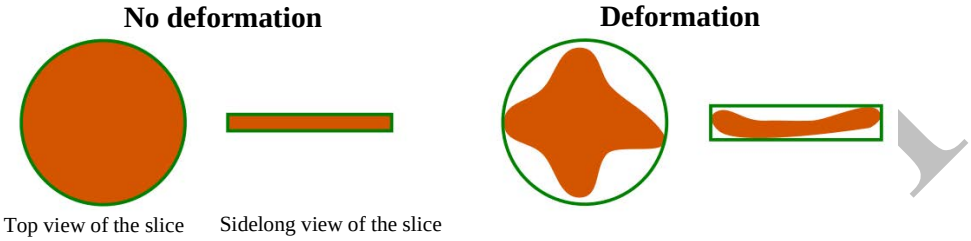

Figure 2: Determination of the deformation.

On the left side, the slice is not deformed. The area of the slice (brown) and the area of its smallest enclosure circle/rectangle (green) is the same which results in a deformation of 1. On the right deformed side, the ratio between the actual slice area and its enclosure circle/rectangle would result in a deformation of less than 1 according the following equation:

$$Deformation(t) = \frac{Area_{slice}(t)}{Area_{enclosure}(t)} \quad (2)$$

2.5 Colour alternation

The colour alternation was measured by reading the colour information of each pixel within the sweet potato slices and averaging it. The obtained RGB values were transformed into the CIE-XYZ colour space according the ISO Standard 13655 which is the base of the CIE-L*a*b* colour space and the Browning Index.
The CIE-L*a*b* colour model was developed with the aim of linearizing the representation of colours with respect to human colour perception and at the same time creating a more intuitive colour system (Burger, 2016). The dimensions in this colour space are the luminosity L* and the two-colour components a*, b*, which specify the colour hue and saturation along the green-red and blue-yellow axes, respectively. The CIE-L*a*b* colour space is often used in literature to describe the colour of food.
The Browning Index is an indicator of the colour change due oxidation of a freshly cut fruit or vegetable surface during storage or drying. The best known and most often quoted Browning Index is a form of excitation purity that follows the suggestion of (Buera, Lozano, & Petriella, 1986) and is expressed as follows (Hirschler, 2016, p. 93):

$$BI = \frac{(x_{D65} - 0.32)}{0.162} * 100 \quad (3)$$

(for Illuminant: D65 and Standard Observer 10°)

where x_{D65} is the CIE Chromaticity value and calculated by the CIE-XYZ values

$$x_{D65} = \frac{X}{(X + Y + Z)} \quad (4)$$

For a more detailed investigation of colour analyses in food processing the interested readers are referred to Martynenko, A., 2017 and Sturm, B. et. al., 2012.

2.6 Moisture Ratio

The moisture ratio was determined according the following equation:

$$X_t = \frac{m_t - m_{dry}}{m_{dry}} \tag{5}$$

Where X_t is the moisture content at any time, m_t the moisture mass at any time and m_{dry} the dry matter which was determined prior to drying. The moisture content (dry base) was then used to calculate the moisture ratio according the following equation:

$$MR = \frac{X_t - X_{EMC}}{X_0 - X_{EMC}} \tag{6}$$

Where X_{EMC} is the equilibrium moisture content which was determined for every test series and X_0 the initial moisture content.

3 Results and discussion

3.1 Weight loss

The weight loss during the drying process is shown in Figure 3.

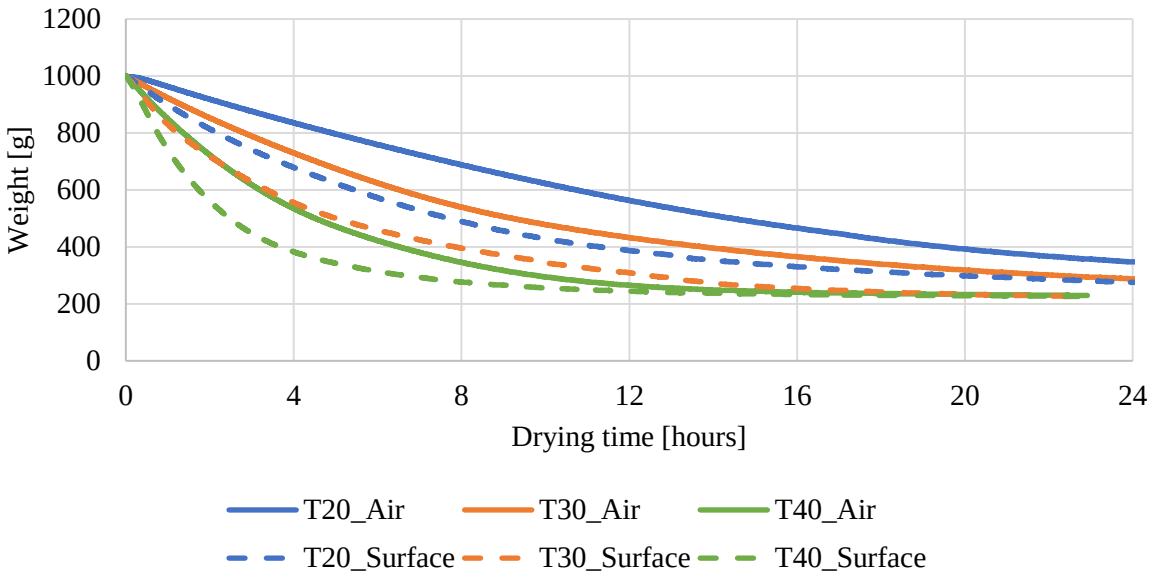

Figure 3: Drying profile by different drying temperatures and methods.

As expected, the drying time is decreasing with higher temperatures. The drying tests where the surface temperature was kept constant are faster since the temperature of the drying air had to be increased as shown in Figure 1. The averaged drying rates during the first drying period are shown in Table 2 below.

Table 2: Average drying rate comparison for the first drying period.

Temperature [C°]	Air temp. controlled [g/h]	Surface temp. controlled [g/h]	Increase factor of drying rate
T_20	41.5	93.0	2.2
T_30	74.0	141.0	1.9
T_40	138.5	219.5	1.5

The surface temperature-controlled method of the lower T20 test series has a drying rate which is approximately 2.2 times higher than the air temperature-controlled method. With higher temperatures, the drying rate factor increases less with ca. 1.9 times for the T30 test series and ca. 1.5 times higher for

the T40 test series. In addition to the drying rate, the ratio of the drying time between the two drying methods was analysed in Figure 4.

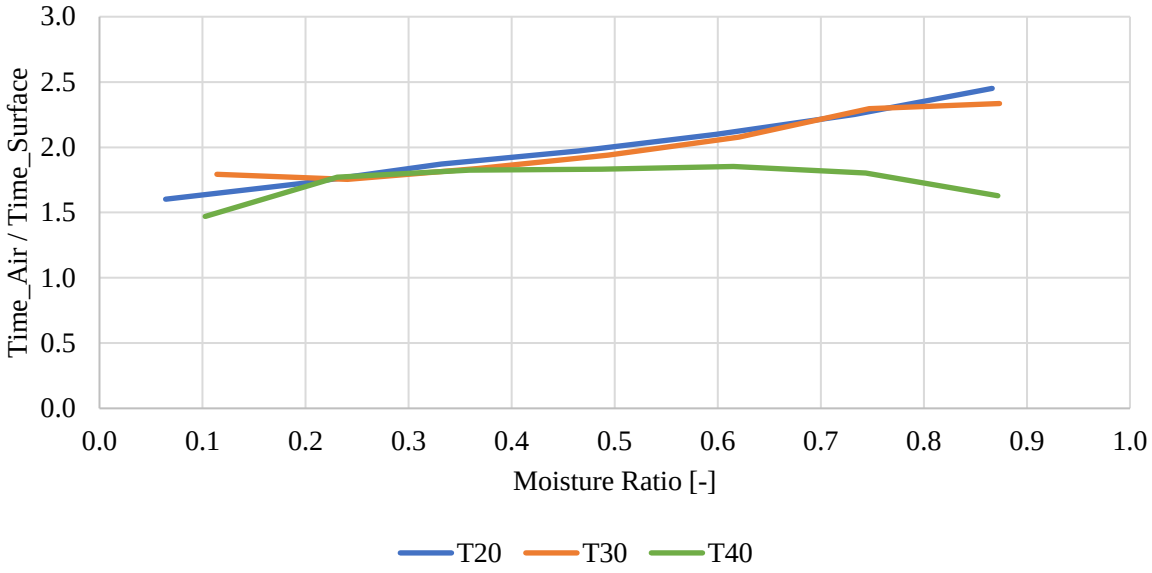

Figure 4: Drying time ratio over moisture ratio.

The results show, that the drying speed factor of the T20 and T30 test series seems to be linear to the moisture ratio. In the beginning of the drying process at a moisture ratio of 0.9 the surface temperature-controlled method is about 2.4 times faster. The factor decreases with the drying process to about 1.6 at a moisture ratio of 0.1. The drying speed ratio of the T40 test series seems rather to be constant over the whole drying process and is between 1.5 and 1.7.

3.2 Shrinkage and deformation

The results of the area shrinkage during the drying process is shown in Figure 5.

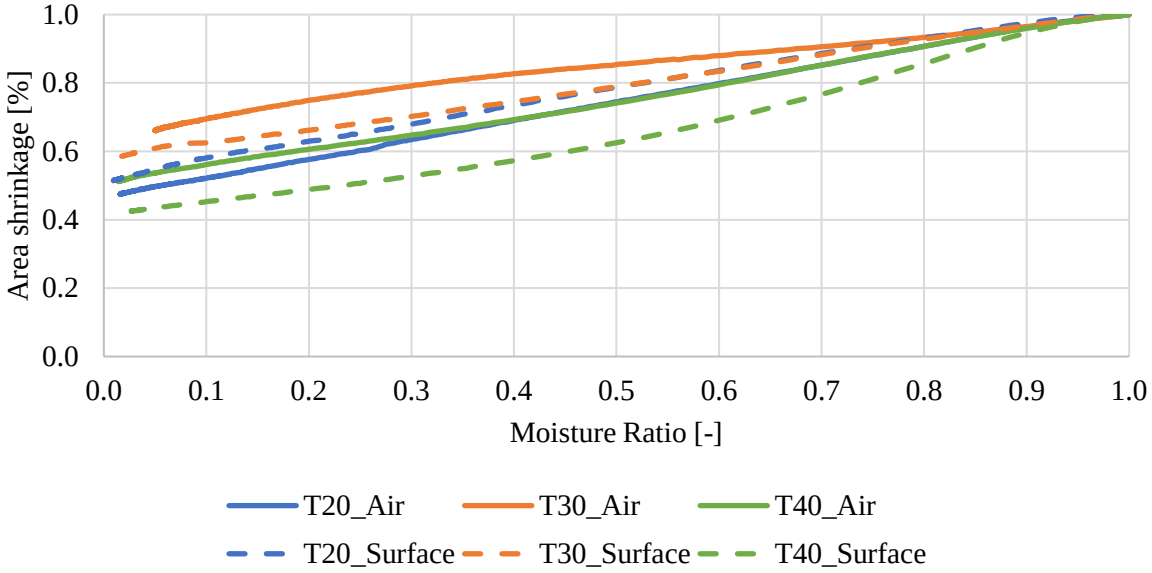

Figure 5: Area shrinkage over moisture ratio.

The result shows an overall area shrinkage of ca. 30% to 60%. The used drying method and drying temperatures doesn't seem to have a significant influence on the shrinkage process. The test series with 30°C result in about 20% less shrinkage compared to the test series with 40°C whereat the surface temperature-controlled method results in a higher shrinkage of approximately 10% compared to its air-

controlled method. The difference of the drying methods of the test series with 20°C is about 0.5% which can be explained that 20°C was very close to the ambient temperature and the temperature difference similar of the drying air temperature of both methods.
The results of the deformation regarding the top view is shown in Figure 6.

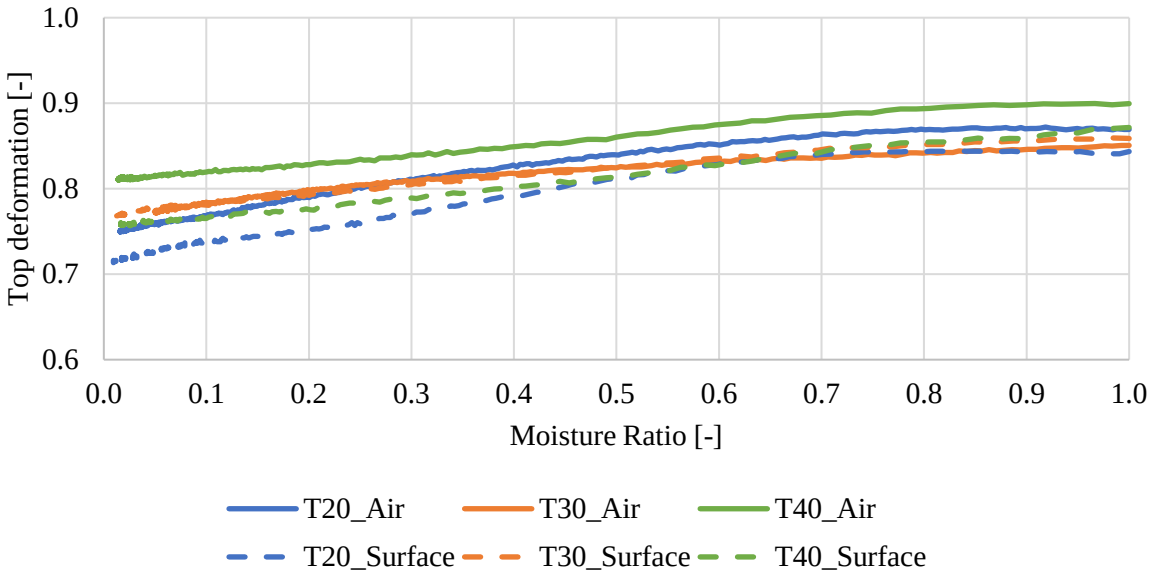

Figure 6: Top view deformation vs moisture ratio.

The chart shows that the deformation progresses of all test series are similar and results in a deformation factor between 0.7 and 0.8. It is not expected that the difference between the single slices regarding to deformation is distinguishable by the human eye. The same behaviour shows the result of the sidelong deformations in Figure 7.

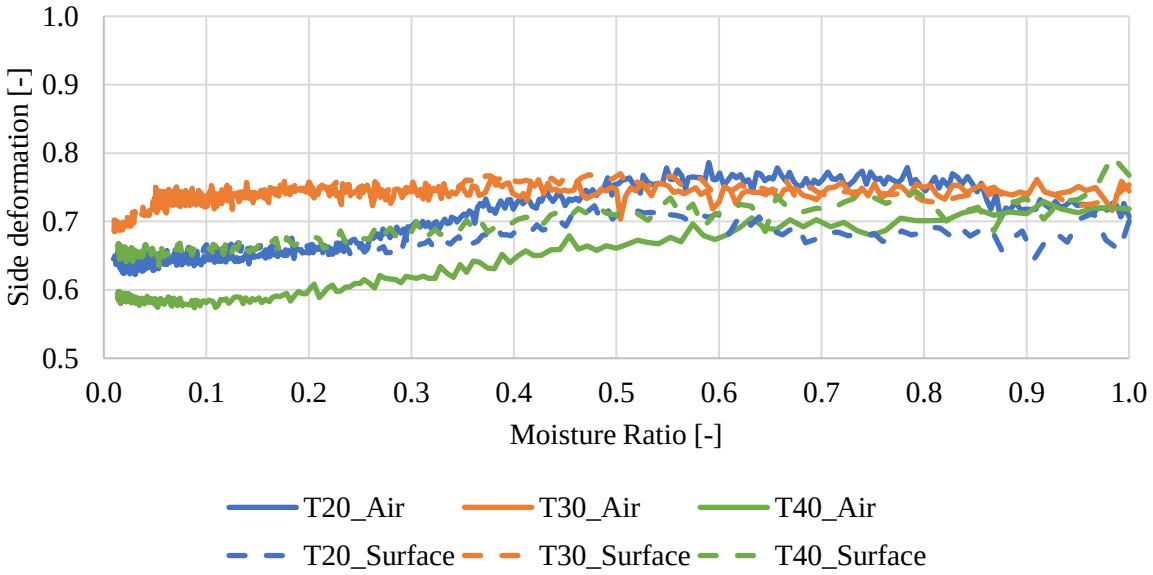

Figure 7: Sideview deformation vs moisture ratio.

The sidelong deformations for all test series are similar and end with a deformation factor between 0.7 and 0.6 what also is not expected to distinguish by the human eye. The deformation during the drying process both top view and the sidelong view seems not to be significantly influenced by the drying temperature and drying method.

3.3 Colour alternation

Th results of the colour alternation during the drying process is shown in Figure 8.

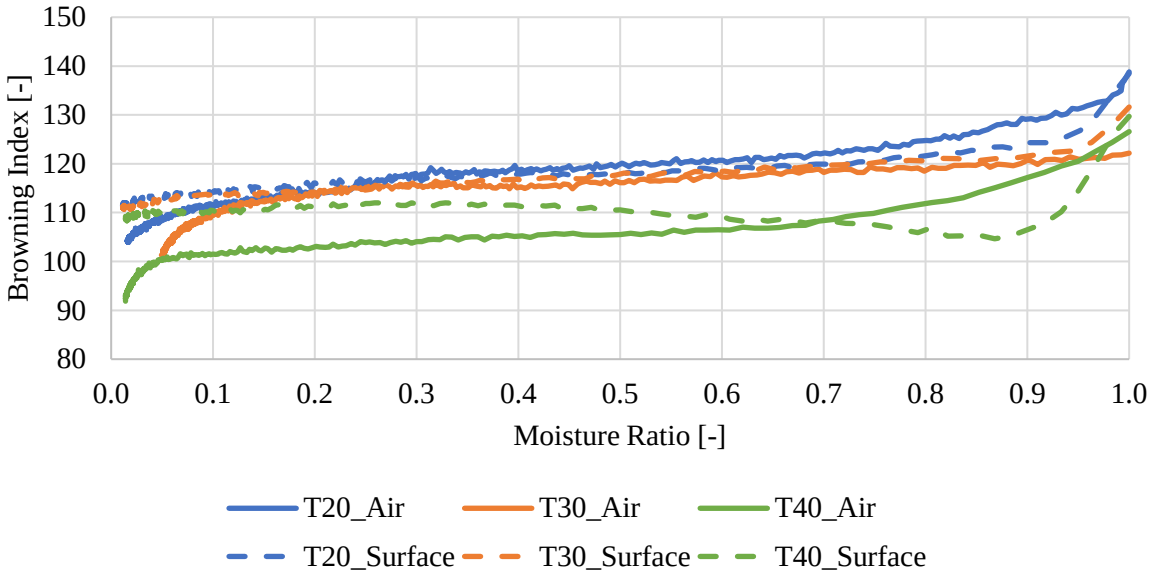

Figure 8: Browning Index vs moisture ratio.

The browning index of all test series is decreasing during the drying process what means that the dried sweet potato slices are perceived as less brown than initially. This can be explained due to the removed water which contributes to a darker, browner perception in the beginning and decreases with the removed water. The difference in browning index between the test series with approximately 20 is rather small and as already at the deformation results, it is not expected that the results are perceivable by the human eye.

4 Conclusions

The results are showing that the drying speed of the constant surface temperature-controlled methods is about 1.5 to 2.5 times faster than the conventional method where the air temperature is kept constant and the optical quality parameters are not significant affected. The area shrinkage at higher temperatures seems to increase about 5% to 10% with the surface temperature-controlled method compared to the air temperature controlled one. The deformation of the top and sidelong view during the drying process doesn't seem to be affected significantly by the temperature and used drying method as well as the colour alternation.

The surface temperature controlled drying method can be used to decrease the drying time without significant negative effects on optical quality parameters like shrinkage, deformation or colour alternation.

5 Nomenclature

BI	Browning Index	-
CIE-XYZ	colour space according the ISO Standard 13655	-
x	Chromaticity value	-

6 Acknowledgement

The work was supported by the Research Council of Norway, grant number 286127 – Core Organic Cofund: SusOrgPlus project as part of the ERA-NET action CORE Organic Plus. The authors acknowledge the financial support for this project provided by transnational funding bodies, being partners of the H2020 ERA-net project, CORE Organic Cofund, and the cofund from the European Commission.

References

Bradski, G. (2000). The OpenCV Library. *Dr. Dobb's Journal of Software Tools*.

Buera, M. P., Lozano, R. D., & Petriella, C. (1986). Definition of colour in the non enzymatic browning process. *Die Farbe*(32), 318-322.

Burger, W. (2016). *Digital image processing : an algorithmic introduction using Java*. New York, NY: Springer Berlin Heidelberg.

Hirschler, R. (2016). Whiteness, Yellowness and Browning in Food Colorimetry. In M. d. P. Buera (Ed.), *Color in Food: Technological and Psychophysical Aspects*.

Martynenko, A. (2017). Computer Vision for Real-Time Control in Drying. Food Engineering Reviews 9(2): 91-111.

Mujumdar, A. S. (2015). *Handbook of industrial drying* (Fourth edition. ed.). Boca Raton: CRC Press, Taylor & Francis Group.

Sturm, B., Hofacker , W.C., Hensel, O. (2012). Optimizing the Drying Parameters for Hot-Air–Dried Apples. Drying Technology 30(14): 1570-1582.